Electrochimica Acta 566 (2026) 148808

Contents lists available at ScienceDirect

Electrochimica Acta

journal homepage: www.journals.elsevier.com/electrochimica-acta

Studying the half-cells' behavior during cyclic voltammetry in $NaNO_3$-KNO_3 melts at 240 °C

Nada Zaghloul [a], Ekin Zehra Metin [a,*], Markus Braun [a], Thomas Bauer [b]

[a] German Aerospace Center (DLR), Institute of Engineering Thermodynamics, Stuttgart, 70569, Germany
[b] German Aerospace Center (DLR), Institute of Engineering Thermodynamics, Cologne, 51147, Germany

ARTICLE INFO

Keywords:
Nitrate melts
Cyclic voltammetry
Electrochemical cell
Gas analysis

ABSTRACT

Thermal Energy Storage (TES) systems, particularly those based on nitrate salts are recognized for their significant potential in supporting intermittent renewable sources. Cyclic voltammetry is a powerful and popular electrochemical technique that could be used to regularly monitor the melt and its corrosive impurities. This research takes a step towards a deeper understanding of the electrochemical reactions of the KNO_3—$NaNO_3$ system by introducing a novel experimental setup that enables optical visualization of both electrodes and distinguishes between the gases produced at each electrode. The formation of the sparingly soluble sodium oxide at the cathodic peak on the working electrode, as suggested in the literature, could be verified through various cyclic voltammetry ranges and also visually confirmed. The dependency of the anodic oxidation reaction on the preceding cathodic reaction and its relation to the electrode surface regeneration has been also verified. Furthermore, this work demonstrates, using the half-cell setup with gas analysis, that NO is produced at the counter electrode during the cathodic peak, whereas the literature so far assumes mainly NO_2 formation. Based on that, a hypothesis suggests that NO and O_2 are produced at the counter electrode during the cathodic peak (**C**), which would behave differently based on the melt composition. On the other hand, no gases are recorded to be produced at the anodic peak(s).

1. Introduction

The growing global emphasis on renewable energy has underscored the critical role of advanced storage technologies in supporting intermittent renewable sources and reducing CO_2 emissions [1]. Among these, Thermal Energy Storage (TES) systems, particularly those based on nitrate salts, are recognized for their significant potential in transitioning former coal-fired power plants into storage facilities and making Concentrated Solar Power (CSP) plants dispatchable [1,2]. Nitrate salts offer several advantages, including low costs, high heat capacity, low vapor pressure, and minimal environmental impact, enabling efficient thermal energy storage at operational temperatures up to 565 °C [1,3].

The reversible reduction of nitrate ions (NO_3^-) to nitrite ions (NO_2^-), shown in Eq. (1), along with oxygen release, is central to the thermal stability of nitrate salt and is influenced by temperature and oxygen partial pressure [4,5]. At higher temperatures, such as above 580 °C, nitrite ions can decompose further, producing oxide species (e.g., O^{2-}) and nitrogen oxide gases (NO_x), which significantly increase the corrosivity of the salt [6,7]. This reaction, shown in Eq. (2), becomes particularly relevant in open systems where nitrous gases are flushed out, preventing stabilization of oxide ion concentrations [6,8]. Corrosion challenges also arise, especially in CSP-TES systems, where molten salt interacts with metal components. Studies report that elevated temperatures lead to the formation of distinct corrosion layers, including sodium-enriched phases and chromium oxides, with basicity levels of the salt playing a pivotal role [9–11].

$$NO_3^- \rightleftarrows NO_2^- + 1/2\ O_2 \quad (1)$$

$$2\ NO_2^- \rightleftarrows O^{2-} + N_xO_y \quad (2)$$

To be able to regularly monitor the salt chemistry, would be very beneficial to TES systems, as this can indicate the presence of unwanted compounds in the system early enough to take respective action as well as indicate plant lifetime expectancy. In-situ electrochemical techniques can be of interest in this case; particularly cyclic voltammetry. This technique is also applied for chlorides [12–14], fluorides [15,16], and carbonates [17].

* Corresponding author at: German Aerospace Center (DLR), Pfaffenwaldring 38-40, 70569, Stuttgart, Germany.
E-mail address: ekinzehra.metin@dlr.de (E.Z. Metin).

https://doi.org/10.1016/j.electacta.2026.148808
Received 10 February 2026; Received in revised form 19 March 2026; Accepted 5 April 2026
Available online 5 April 2026

Cyclic voltammetry is a powerful and popular electrochemical technique commonly employed to investigate the reduction and oxidation processes of molecular species. A cyclic/varying potential is imposed on the system and the resultant current is measured. As the potential is scanned negatively (catholically), a reduction reaction takes place and appears as a peak in the current curve. When the scan direction is reversed, and the potential is scanned in the positive (anodic) direction, an oxidation reaction occurs, which can also be detected as a peak [18]. In this sense, cyclic voltammetry could be potentially used to detect impurities in the salt, through the new peaks that can appear during the scan, and they can also be quantified through the peak intensity. However, it is important to have a better fundamental understanding of the cyclic voltammetry operation window of nitrate melts before proceeding with identifying impurities.

In the case of nitrate salt, most of the electrochemistry research was done between the 1960s to the 1990s with a limited number of publications. The process responsible of giving a rise to a cathodic current is well studied in literature and is known to be the result of nitrate ion reduction as per Eq. (3) [19–24]. It is often suggested that the produced oxide forms a metal oxide layer on the electrode surface which then is oxidized during the anodic sweep [20,21,23].

$$NO_3^- + 2\,e^- \rightarrow NO_2^- + O^{2-} \quad (3)$$

Moreover, Swofford et al. studied the effect of adding nitrite and oxides to eutectic potassium and sodium nitrate and could detect on the current-voltage diagram changes between the sweeps according to the added concentration [25]. Bartlett et al. had a study on the cathodic process in molten nitrates and nitrites and suggested multiple half-cell reactions, with their respective overall cell reactions [19]. Miles et al. studied the effect of the metal cation on the cyclic voltammetry and suggested that the cation has a catalytic effect on the reduction reaction [21]. Villard et al. deduced a reaction pathway for the electrochemical oxidation of oxide anions at a platinum electrode in molten $NaNO_3$ from the analysis of cyclic voltammograms [22]. Singh et al. studied the cyclic voltammetry behavior in dried and wet nitrate melts and the catalytic effect of water on nitrate ion reduction in the wet melt.

Recently, the research about this topic has become very scarce, and to be able to apply this electrochemical technique to today's potential applications, further fundamental understanding is of vital interest. It is therefore the aim of this paper to revive and further deepen the fundamental research of cyclic voltammetry in nitrate melts. The gases produced during the measurements have been rarely studied, although they can help identifying the reactions at the electrodes. To the best of our knowledge, there was no research focused on the visibility of gases produced at the electrodes and their subsequent analysis. Moreover, the focus has usually been on the working electrode only, which omits the events happening at the counter electrode. This research takes a step towards a deeper understanding of the electrochemical reactions of the KNO_3–$NaNO_3$ system by introducing a novel experimental setup that enables optical visualization of both electrodes and distinguishes between the gases produced at each electrode. The research aims to validate and, where necessary, update previous findings in this field.

2. Materials and methods

2.1. Experimental setup

Fig. 1 shows a schematic of the experimental setup used for the experiments. A test rig with two half cells made from polyetheretherketon (PEEK) was loaded with 12 g of nitrate salt. PEEK was chosen to avoid any side-reactions of the molten salt with the cell, electrically insulate the system, as well as for the ease of machining the necessary cell design. To stay within the comfortable thermal stability limit of the PEEK material, the experiments were conducted at 240 °C salt temperature. Eutectic Salt (50 mol% $NaNO_3$, 50 mol% KNO_3) was produced by the mixing of $NaNO_3$ (Merck, purity > 99%) and KNO_3 (Merck, purity > 99%). An amount of Nitrite ($NaNO_2$, Merck, > 99%) contributing to 5 mol% of total salt anion fraction was used in some experiments. Before the experiments, both the salt and the PEEK cell were preheated to 300 °C at a heating rate of 2 K min^{-1} to ensure the removal of moisture.

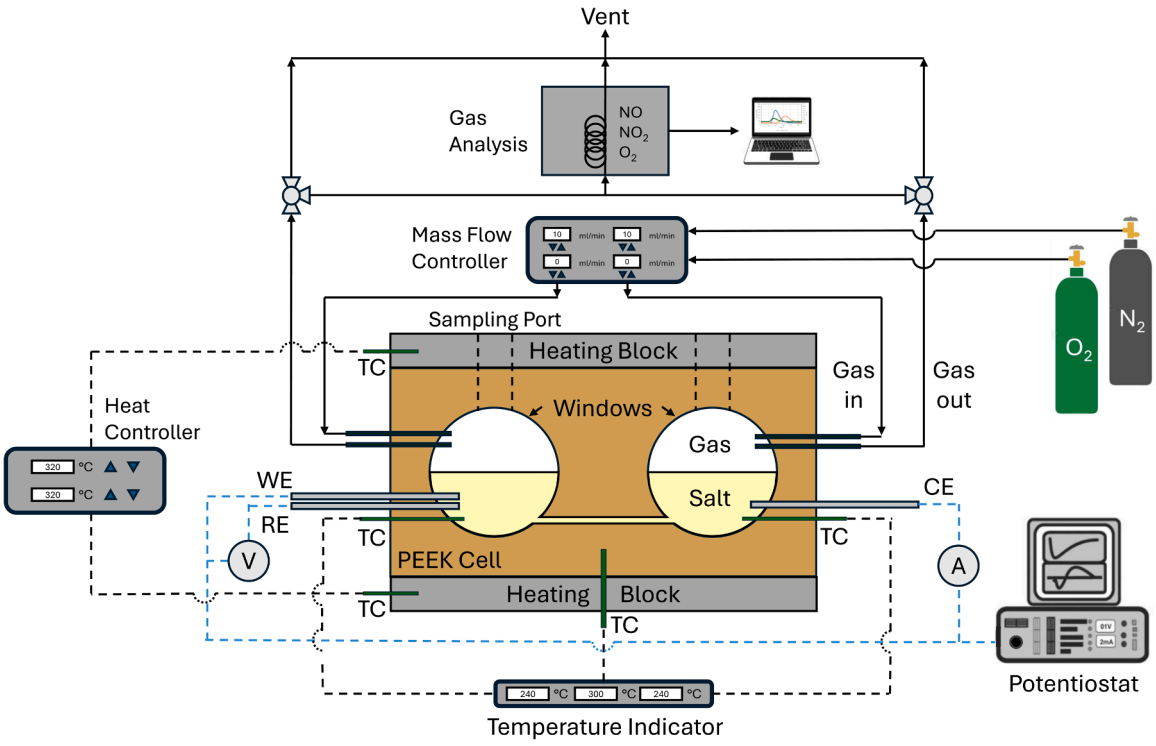

Fig. 1. Schematic of experimental setup for CV measurements in molten nitrate salt: WE – working electrode, CE – counter electrode, RE – reference electrode, and TC – thermocouple.

The electrochemical cell, which was heated using heating cartridges, offered a view into the salt through sapphire windows for each half cell (Fig. 1). The two half cells – each approximately 7.8 cm^3 in volume with a cross-sectional diameter of 1.8 cm and 3 cm depth - were connected through a 2 mm diameter hole passing through the PEEK. Moreover, each half-cell volume included a K-type thermocouple, gas inlet, gas outlet, sampling port, and electrode(s). To fix the atmospheric composition, the volume was purged on top of the salt with a constant gas flow of 10 mL/min in each half-cell. The gas composition was varied across the experiments but the gases used in general are N_2 and O_2 (both 5.0 grade, Linde gas, Germany) regulated by digital mass flow controllers (EL-FLOW Prestige, Bronkhorst).

Three platinum rods of 2 mm diameter were inserted from the sides into the molten salt to be used as the electrodes. Platinum was selected as electrode material as it is known to be stable in nitrate salt environment and would therefore unlikely affect the measurements. The geometric surface area of both the working electrode (WE) and counter electrode (CE) was 0.257 cm^2, and all current values were normalized accordingly to obtain current densities (mA cm^{-2}). The working and a reference electrode were at one side of the cell, while the counter electrode was at the other half cell. In previous research in the literature, an Ag/Ag^+ – usually a silver wire in a melt containing $AgNO_3$ – was used as a reference electrode [20,21,25]. In this research, for a higher durability of the electrode, the platinum quasi-reference electrode was used. According to Manning, half-wave potentials referenced to the quasi-reference electrode are inherently arbitrary; nonetheless, they are reproducible and therefore particularly useful for studies involving corrosive melts [26]. The electrochemical cell was connected to a Metrohm Potentiostat (PGSTAT 204) for applying the potential in the cathodic and anodic direction, and measuring the flowing current as a result.

2.2. Analysis methods

In this work, multiple analytical methods were applied, and their results were correlated. These methods — cyclic voltammetry, visual inspection by camera, salt analysis and gas analysis — are briefly introduced below.

2.2.1. Cyclic voltammetry

Cyclic voltammetry in this research served as the experimental procedure by applying the potential sweep. Nevertheless, it also served as analysis method, as the resulting current studied represents electrochemical activity in the melt. For measurements at 240 °C, a scan rate of 500 mV/s was selected, as preliminary experiments (not shown) demonstrated that it provides well-defined and reproducible peaks, enabling reliable identification of the redox couples. For every measurement, the potentiostat was set to perform three sweeps within the designated potential range with a scan rate of 500 mV/s. All sweeps were included in the analysis and the purpose of multiple sweeps is to compare the cycles and deduce conclusions from their behavior. All electrochemical measurements were conducted without iR compensation, and the potential values reported are therefore not corrected for uncompensated resistance. The generation of peaks and/or limiting currents (at the end of the electrochemical window) were correlated with the other analysis methods described in this section.

2.2.2. Visual inspection by camera

During the measurement each chamber was recorded by a Camera (Nikon D3500) positioned in front of the half-cell window to correlate activity at the electrode in the salt melt with the respective potential in the sweep. This served the purpose of identifying at which sections of the CV plot gases are produced or electrode surface is affected.

2.2.3. Salt analysis

Over the course of the experiments, which will be described in Section 2.3, salt samples were extracted and analyzed by wet chemistry to monitor salt composition. The samples were first analyzed using ion chromatography (IC) (Metrohm model 880 Basic IC plus, Switzerland) for nitrate and nitrite ions. Ion chromatography was performed using a mobile phase consisting of 4 mM Na_2CO_3 and 1 mM $NaHCO_3$. Calibration was carried out using multi-ion standard solutions. Nitrate was calibrated using four standards (19–190 mg L^{-1}, $R^2 = 0.99996$), and nitrite using five standards (0.06–6 mg L^{-1}, $R^2 = 0.99991$). For ion chromatography 125 mg of salt was dissolved in 500 ml ultra-pure water and analyzed. The oxide ion contents were determined by automated acid base titration (Metrohm Titrando 800, Switzerland) under an inert purge gas of Ar (5.0-grade Linde gas). This technique is based on the reaction of basic oxide ions (e.g., O^{2-}) in water to form two hydroxide ions (HO^-). The amount of hydroxide ion can be determined by titration with HCl solution (0.01 M) until neutrality. Based on the hydroxide amount, the total oxide content is calculated. This method does not allow for differentiation between the types of oxides present, for example O^{2-}, O_2^{2-}, or O_2^- [27].

2.2.4. Gas analysis

The outlet gas, which carried the gases produced during the measurement was passed through a gas analysis (Xstream, Emerson), which detects NO and NO_2 up to 2000 ppm as well as O_2 in volume percentage. The transit time for gas produced in the cell to reach the gas analysis system was approximately 1 min. Consequently, the measured gas composition represents an accumulation over the duration of the electrochemical measurement rather than instantaneous gas evolution. The separate gas chambers in the cell design, allow for separate analysis of the gases at each half-cell and hence provides better insights into the phenomena. To achieve this, each electrochemical measurement was performed twice to alternate between the half-cells, where one is sent to the gas analysis and the other to the vent.

2.3. Experimental matrix

The main parameters varied were salt composition, gas composition, and the CV voltage sweep range. The CV voltage sweep range, in particular, defines the three categories into which the measurements in this study are grouped (Table 1). Moreover, the exchange of the salt in the cell is indicated in the table as salt batches. Fig. 2 elaborates the experiments' names that will be referred to throughout the paper.

The first category (FV) comprises full cyclic voltammetry sweeps to the cathodic and anodic limits, comparing the influence of salt composition and cover gas. This category includes four systems in which both the salt composition and the cover gas are varied. The second category (LV) is a limited section of the complete voltage sweep range. This sweep

Table 1
Experimental matrix details.

Experiment Name	Category	Salt	Overhead Gas	Salt Batch
FV_Eu_N2	FV	50/50 mol% - $NaNO_3$ / KNO_3	100% Nitrogen	A
FV_Eu_O2N2	FV	50/50 mol% - $NaNO_3$ / KNO_3	50% O_2 – 50% N_2	B
FV_Nit_N2	FV	5/45/50 mol% - $NaNO_2$/$NaNO_3$ / KNO_3	100% Nitrogen	C
FV_Nit_O2N2	FV	5/45/50 mol% - $NaNO_2$/$NaNO_3$ / KNO_3	50% O_2 – 50% N_2	D
LV_Eu_N2	LV	50/50 mol% - $NaNO_3$ / KNO_3	100% Nitrogen	A
LV_Nit_N2	LV	5/45/50 mol% - $NaNO_2$/$NaNO_3$ / KNO_3	100% Nitrogen	C
CoV_Eu_N2	CoV	50/50 mol% - $NaNO_3$ / KNO_3	100% Nitrogen	E
CoV_Nit_N2	CoV	5/45/50 mol% - $NaNO_2$/$NaNO_3$ / KNO_3	100% Nitrogen	F

Fig. 2. Nomenclature of the experiments.

range covered the following three sections: LV.a - the cathodic peak range, LV.b - the anodic peak(s) range, and LV.c - the cathodic and anodic peaks excluding the electrochemical limits. More LV ranges were also measured and are described in the supplementary materials in Table S1. This will be elaborated further in the results section. The third and final category of the measurements (CoV) is the constant potential measurement. During these measurements the potentiostat applies the cathodic and anodic peak potential for 30 s. The second and third categories each include two systems, in which two salt mixtures were examined under a nitrogen atmosphere.

3. Results and discussion

The following three subsections address the electrochemical measurements with visual observations, as well as salt and gas analysis (Section 3.1 - FV), (Section 3.2 - LV), and (Section 3.3 - CoV).

3.1. Complete cycle comparison (FV)

3.1.1. Overall cyclic voltammetry analysis

Fig. 3 presents a cyclic voltammetric curve recorded within a voltage window of −3 V to 2 V vs. the quasi-reference electrode with and without nitrite in the salt under nitrogen atmosphere.

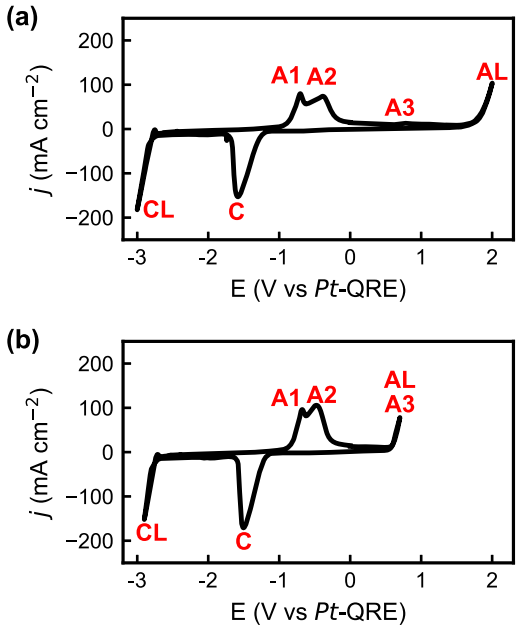

Fig. 3. Cyclic Voltammetry of (a) Eutectic Nitrate Salt (FV_Eu_N2) and (b) 5 mol% Nitrite Salt (FV_Nit_N2) at 240 °C under Nitrogen atmosphere using three platinum electrodes.

A well-defined cathodic peak (**C**) is to be seen at the potential of −1.6 V. According to literature the cathodic current related to this peak is attributed to the alkali metal oxide formation at the electrode surface as described by Eq. (3) followed by Eq. (4) [23].

$$O^{2-} + 2\ Na^{+} \rightarrow Na_2O\ (solid) \tag{4}$$

During the anodic scan, two anodic peaks appear between −1 V and 0 V (**A1** & **A2**). The anodic peaks of the cyclic voltammetry are believed to be related to the oxidation of the metal oxide formed during the cathodic reduction peak [20,21,23]. Singh et al. assigned the first anodic peak to the potassium molecule and the second anodic peak to the sodium molecule [20]. In the case of the potassium cation, when K_2O is produced, K_2O is expected to be rapidly converted to KO_2; therefore, the species proposed to undergo oxidation is KO_2 [20]. Accordingly, **A1** should correspond to Eq. (5) and **A2** to Eq. (6) [20].

$$KO_2 \rightarrow K^{+} + O_2 + e^{-} \tag{5}$$

$$Na_2O\ (solid) \rightarrow 2\ Na^{+} + 1/2\ O_2^{-} + 1.5\ e^{-} \tag{6}$$

The cathodic and anodic limits (**CL** and **AL** in Fig. 3) are less frequently studied in literature. Villard et al. [22] and Miles et al. [21], stated that the Anodic Limiting (**AL**) current (at 2 V for the case FV_Eu_N2) is related to the nitrate oxidation reaction into NO_2 and O_2 shown in Eq. (7). Moreover, they suggest that an earlier oxidation peak (defined as Peak **A3** at 0.8 V in the presented work) is the nitrite oxidation peak, also producing NO_2 as presented in Eq. (8). The peak is very small in the case of the eutectic melt, as the nitrite amount present is only that produced by the cathodic sweep as per Eq. (3).

$$NO_3^{-} \rightarrow NO_2 + 1/2\ O_2 + e^{-} \tag{7}$$

$$NO_2^{-} \rightarrow NO_2 + e^{-} \tag{8}$$

When comparing the CV curve of the eutectic mixture to that of the 5 mol% nitrites, one would notice that they are almost a match, except for when 5 mol% of nitrites are added to the eutectic mixture the anodic limit is shifted from 2 V to 0.8 V (Fig. 3(b)), as the nitrite peak dominates the anodic limit. Miles et al., also noticed that as the temperature increases and the nitrite concentration increases due to the thermal decomposition, the nitrite oxidation peak increases such that it dominated the anodic reactions [21]. Similarly, the same effect can be considered when nitrite is deliberately added to the melt.

3.1.2. Visual inspection of activity corresponding to CV

The newly developed setup within this work provides an opportunity to have an instant visual view at the electrodes during the cyclic voltametric measurement and study the activity around them. An activity can be referring to gas production and/or formation or dissolution of potentially solid compounds near the electrode. As the potential sweep starts in the cathodic direction then the anodic direction, the images' results will be presented in the same order for each electrode, starting

with the working electrode and then the counter electrode.

For the working electrode side, shown in Fig. 4, the thermoelement (silver in appearance and located lower in the image) and the reference electrode (slightly out of focus), are visible in the background. The difference can be seen between the working electrode's fresh state before any potential is applied (top left), and the state at the cathodic peak (**C**) during the sweep (top right), where it appears less shiny. No further activity near the electrode is noted when the sweep reaches the cathodic limit (**CL**). When the sweep reaches the anodic peak (**A1 & A2**), a white colored material rises from the electrode (bottom left). Finally, at the anodic limit (**AL**), excessive gas production can be visually detected.

Fig. 5 shows the counter electrode (appears white), with the thermoelement (silver) in the background. During the cathodic peak (**C**) gas is produced at the counter electrode (left). The same can be noted for the cathodic limit (**CL**), whereas the amount and intensity of gas production is much higher for the cathodic limit (right). No Activity is seen during the sweep in the anodic direction (**A1, A2 & AL**).

It was noted during the measurement, that activity at the working electrode is visible during the sweep in the cathodic as well as anodic direction with different characteristics of the activity. What can be seen at the working electrode supports the literature suggestion of the formation of a metal oxide on the electrode during the cathodic peak (Fig. 4, top right), which then oxidizes at the anodic peak (Fig. 4, bottom left) [20]. Meanwhile, all activities at the counter electrode correspond to elements of the CV curve during the cathodic sweep only (for the anodic sweep there was no activity at the counter electrode). The process occurring at the counter electrode, however, is rarely studied in detail. For this reason, particular emphasis is placed on the counter electrode in this research. Having established that electrochemical activity occurs at both electrodes, analysis of the produced compounds will provide further insight into the underlying phenomena. This analysis is presented in the following sections.

The visual inspection showed the same results for LV and CoV experiments, so the SubSections 3.2 and 3.3 will not include additional images. Yet in the occasion a difference is observed, it is stated accordingly.

3.1.3. Salt analysis

One purpose of the two–half-cell setup is to enable identification of the chemical compounds produced as a result of the electrochemical reactions near each electrode, by allowing individual salt samples to be extracted from each chamber. This should provide a better understanding of the reaction mechanism during the cyclic voltammetry. As can be seen in the experimental setup in Fig. 1, the gas chambers are physically separated in the design. Nevertheless, the salt chambers are connected by a bridge (2 mm diameter, 20 mm length), which enables electrochemical measurements while limiting ion diffusion between the chambers, thereby allowing individual salt sample analysis from each chamber.

In all cases discussed in this work, salt samples from each chamber resulted in similar composition for all the batches described in Table 1. Traces of nitrite and oxide(s) could be detected on both sides. It appears, that by the time the sample was taken, diffusion had already occurred. The amount produced is a function of the number of sweeps performed before the samples are taken. Hence, one could suggest that, the higher the number of sweep cycles, the higher the production of ions in the melt, which could potentially overcome the diffusion rate across the cells and then a difference in salt chemistry can be detected. Similar to the visual inspection, the results for the salt analysis for FV category did not differ from the other two categories, hence they will not be discussed further.

3.1.4. Gas analysis combined with cyclic voltammetry analysis

Unlike the salt analysis, the gas analysis led to valuable results, as there is no connection between the gas chambers and each gas region has its own gas inlet and outlet towards the gas analysis. Moreover, the gases produced are analyzed continuously during the measurements and can therefore be associated with individual experiments/measurements. Yet, note that these produced gases are a result of the complete cycle and do not represent a single event during the sweep, but an overall gas production.

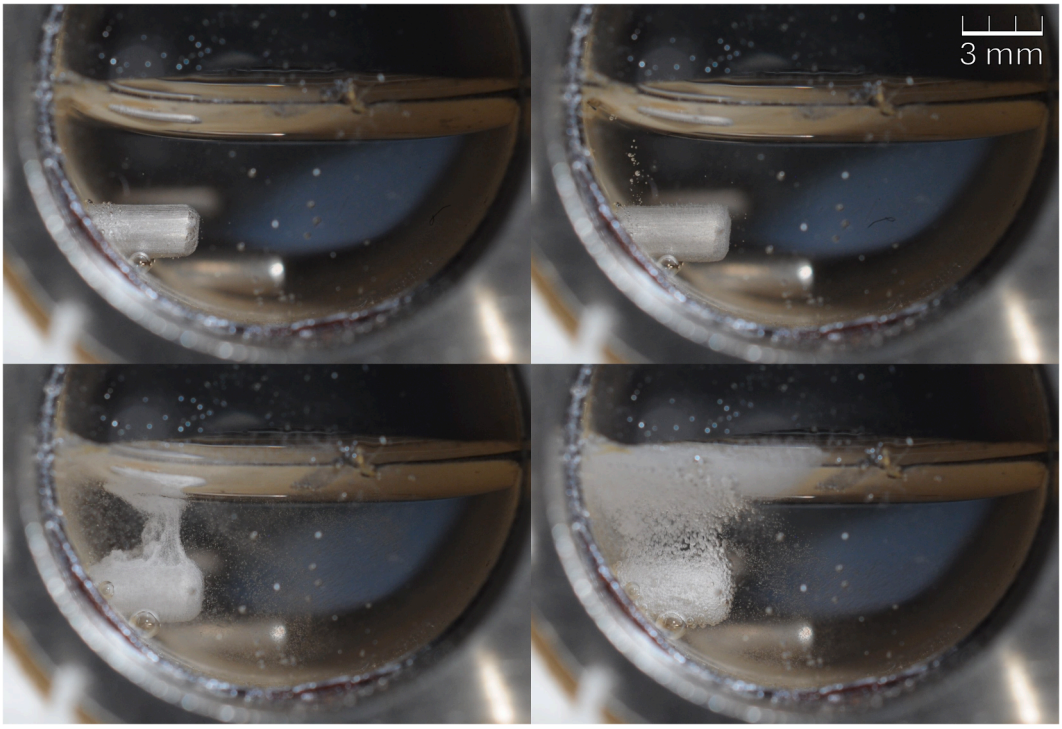

Fig. 4. Images of the **working electrode** during a cyclic voltammetry (FV_Eu_N2) at different moments: without potential with fresh electrode (top left), cathodic peak (**C**) (top right), anodic peaks A1, A2, A3 (bottom left), and anodic limit AL (bottom right).

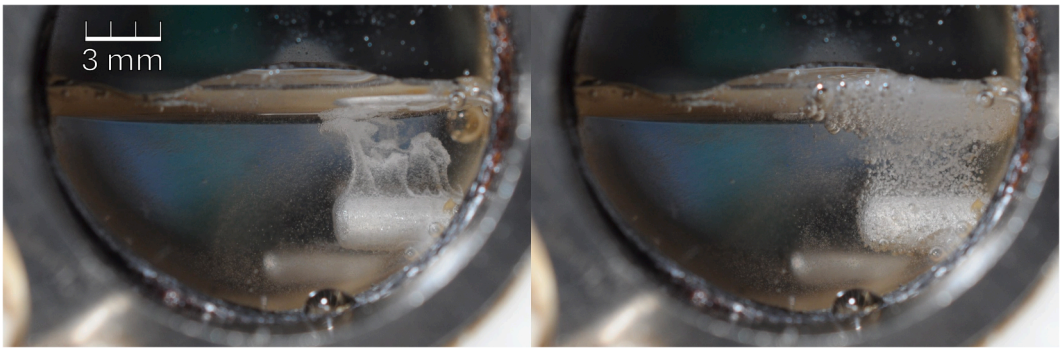

Fig. 5. Images of **counter electrode** during cyclic voltammetry (FV_Eu_N2) at different moments: cathodic peak C (left) and cathodic limit CL (right).

This section focuses on comparing the gas production across the various experiments described in the experimental matrix for the full cycle experiments (Table 1, Category: FV). The set of measurements were designed to compare the products appearing in the gas analysis for the different salt and gas compositions. The comparison for FV category is depicted in Fig. 6. It should be noted though that occasionally at the beginning of the plots there is a step up or down for the oxygen concentration, this should not be mistaken for a peak. In fact, even when flowing 100% nitrogen, a zero offset remains in the gas analysis, and this offset differs between chambers. Consequently, when the valve is switched to the chamber of interest, the zero offset changes and then stabilizes over time. Only in the presence of actual oxygen production does a true peak appear in the gas analysis plot, rather than a simple step increase or decrease.

The first point to be noted here, is that the only difference between the cyclic voltammetry of all four systems, is that when nitrite is present, the anodic limit appears at a lower potential; in this case 0.8 V instead of 2 V. No new peaks appear in the curve. Nevertheless, the gas analysis differs to a great extent.

For the first case - the eutectic salt under nitrogen atmosphere (Fig. 6

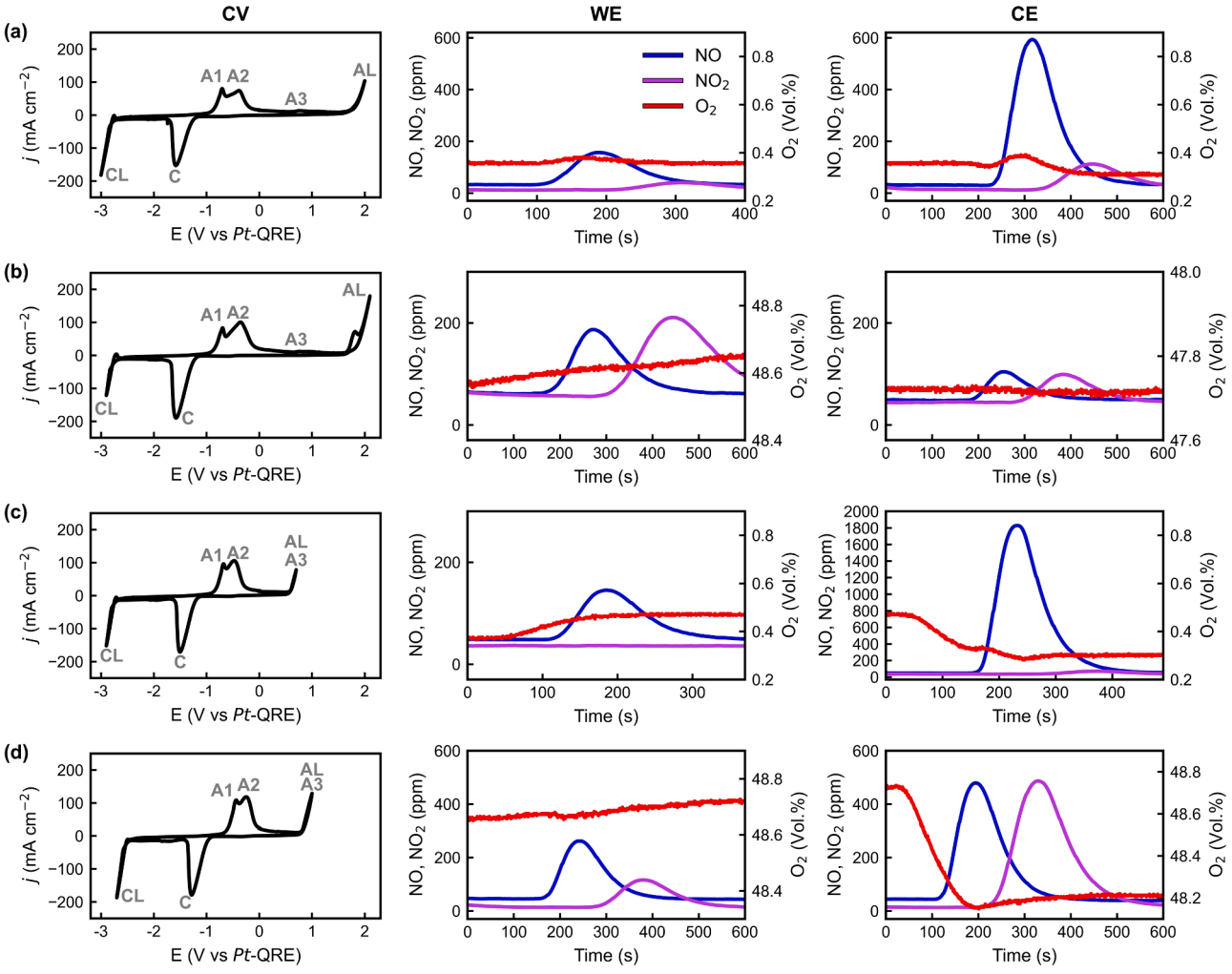

Fig. 6. Cyclic Voltammetry (left) and gas analysis (middle and right) over the full potential range (−2 V to 3 V, Cat. FV) for the following four salt and gas compositions: (a) FV_Eu_N2, (b) FV_Eu_O2N2, (c) FV_Nit_N2, (d) FV_Nit_O2N2.

(a)) NO, NO_2 and possibly O_2 are produced, while NO production is higher than NO_2 production. The following relation between changes of the salt and/or gas atmosphere to the NO_2 is to be noticed at the working as well as the counter electrode. When the gas atmosphere is changed to include 50% O_2 (Fig. 6(b)), the NO_2 production increases relative to the NO production. When nitrite is added to the melt, under nitrogen atmosphere (Fig. 6(c)), NO_2 is no longer detected in the gas analysis. However, when oxygen is introduced to the gas atmosphere, NO_2 is detected again in the gas analysis (Fig. 6(d)).

As no new or distinct peaks appear in the CV curves upon changing the salt composition and/or gas atmosphere, the observed differences in gas production are most likely the result of chemical reactions rather than electrochemical processes. In particular, the only observable change occurs at the anodic limit, which in both cases is expected to produce NO_2 as per Eq. (7) or Eq. (8) and thereby should not affect the presence of NO_2. This will be discussed further in Section 3.4. Nevertheless, analyzing the results of a complete cycle is limiting the possibility of assigning the gases produced to particular peaks. Therefore, the system will be analyzed deeper by omitting the limits and isolating the relevant peaks of interest for this research, which is the second category of experiments.

3.2. Isolated peaks (Category LV)

3.2.1. Cyclic voltammetry analysis

Another advantage of studying limited potential ranges, other than assigning the gas products to the peaks, is the ability to investigate peak dependencies to validate literature suggestions. The potential ranges of interest in this research are the ones that cover the isolated cathodic reduction peak (**C**) (LV.a), the isolated anodic oxidation peak(s) (**A1-A2**) (LV.b) and the range covering the cathodic and anodic peaks (**C- A1-A2**) (LV.c). The salt composition was a variable parameter (sodium/potassium nitrate eutectic salt and the nitrate eutectic + 5mol% nitrite). For all LV category experiments, the chosen gas environment is the nitrogen atmosphere to have a higher sensitivity for the oxygen production. The resulting CV curves along with the gases produced at each electrode are presented for eutectic nitrate salt (Fig. 7) and eutectic nitrate salt with nitrite addition (Fig. 8).

The first notable observation from Figs. 7 and Fig. 8 concerns the shape of the CV curves. The gas analysis is discussed in Section 3.2.2. It should be noted that the discussion of the CV results for Figs. 7 and Fig. 8 is combined, as both figures show identical behavior.

For both salt melts, when the potential range is set to only cover the range of the cathodic peak (−2 V to −1 V), the peak appears during the first sweep and does not appear again during the two subsequent sweeps. On the other hand, when the potential range is set to only cover the range of the anodic peaks (−1 V to 0,2 V), the anodic peaks do not appear at all and the current stays zero across the three sweeps. Finally, when the range is combined to cover both ranges (−2 V to 0,2 V), there are multiple observations.

1. The CV curve shows peaks in the cathodic as well as the anodic range.
2. The two anodic peaks previously seen during the complete sweep in SubSection 3.1 appear now to be only one single peak most likely corresponding to peak **A2**, due to the position of the tip.
3. Both anodic and cathodic peaks appear during all three sweeps, and the second and third sweep produce larger peaks than the first sweep.

It is concluded that the cathodic peak appears only during the first cycle of the cathodic sweep LV.a, due to the deactivation of the working electrode by the produced solid Na_2O which precipitates on its surface due to its low solubility [21,23]. On the other hand, the redissolution process described in Eq. (9) below is sufficiently fast to accelerate the physical redissolution in the melt of the Na_2O accumulated on the working electrode, due to the higher solubility of Na_2O_2 [20,21,23,28,29].

$$O^{2-} + NO_3^- \rightleftarrows O_2^{2-} + NO_2^- \quad (9)$$

This phenomenon, suggested in literature, has been validated also in

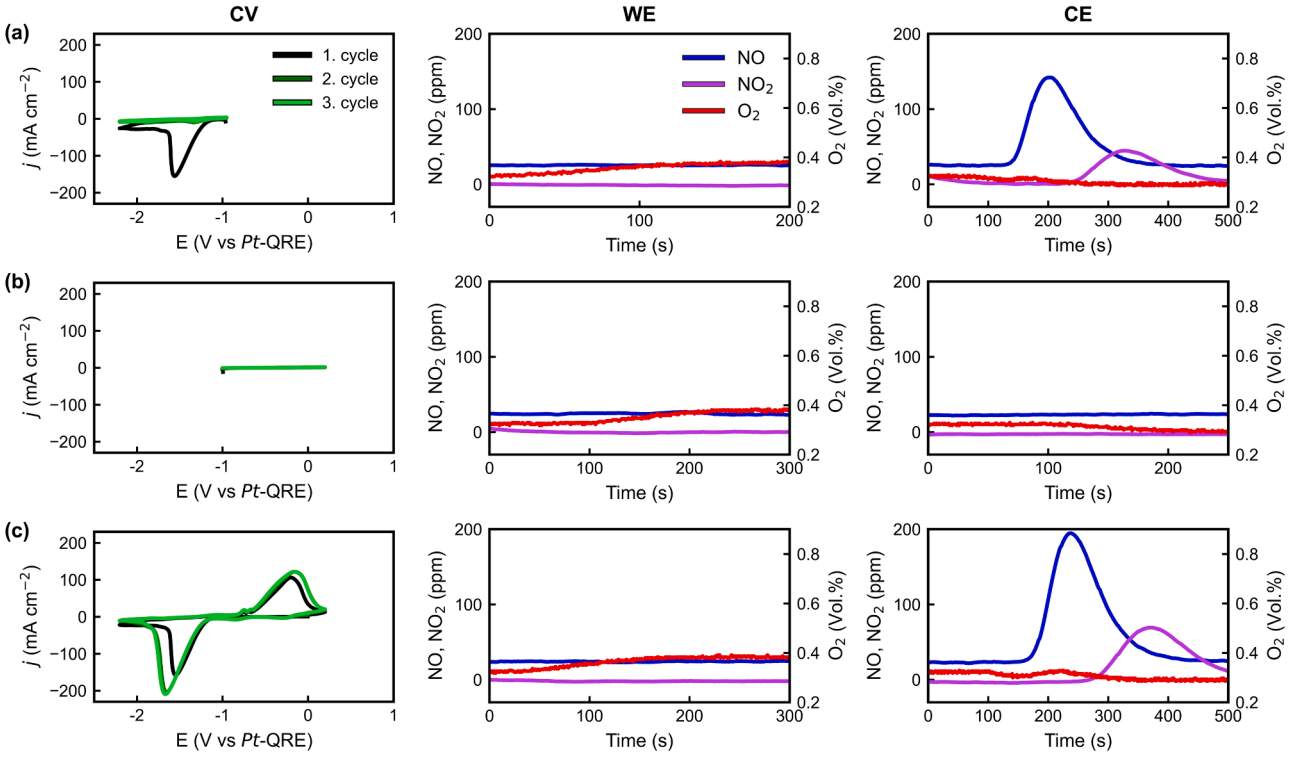

Fig. 7. Isolated CV sections (left) with their respective gas analysis for the working electrode (middle) and counter electrode (right) for eutectic salt under nitrogen atmosphere (LV_Eu_N2). The voltage window was set for (a) cathodic peak, (b) anodic peak, and (c) cathodic + anodic peak.

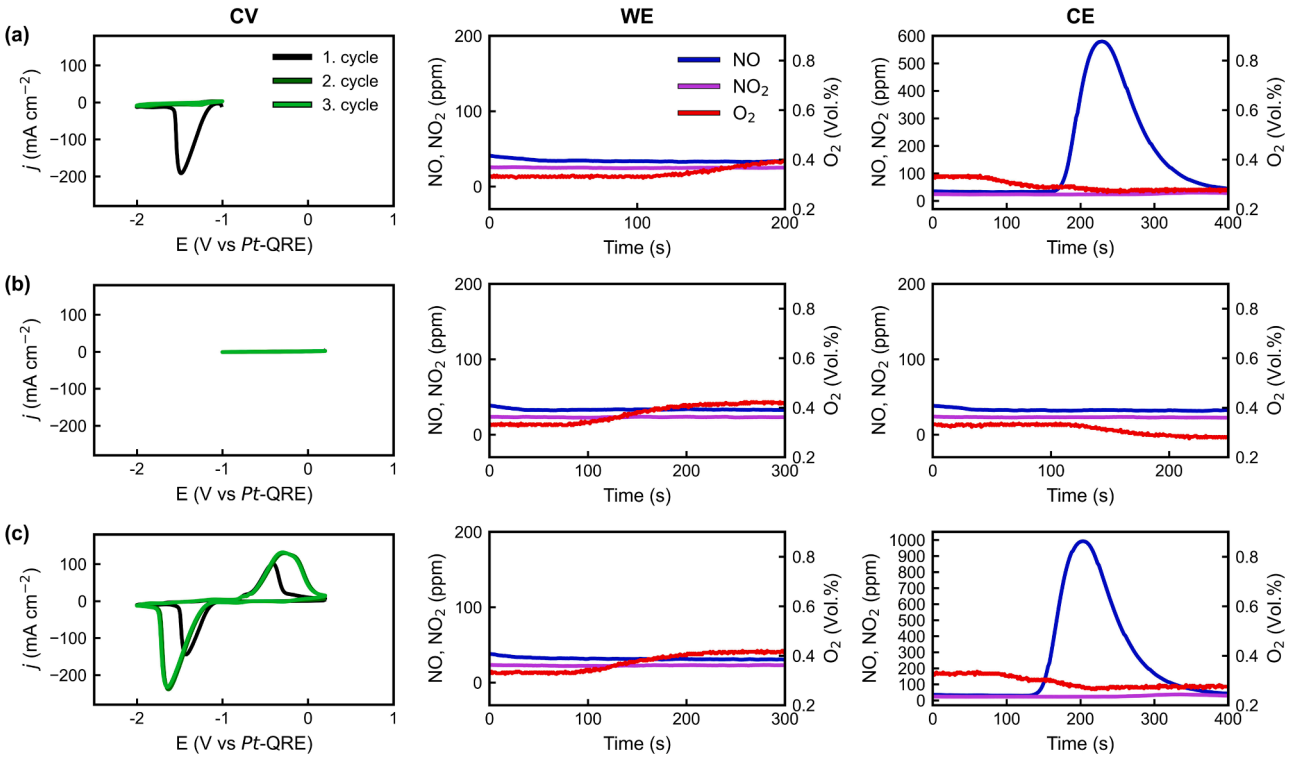

Fig. 8. Isolated CV sections (left) with their respective gas analysis for the working electrode (middle) and counter electrode (right) for eutectic salt under nitrogen atmosphere (LV_Nit_N2). The voltage window was set for (a) cathodic peak, (b) anodic peak, and (c) cathodic + anodic peak.

this research, by repeating the measurement a few minutes later. It was noted that the cathodic peak (**C**) would reappear during the first cycle. This means that the reason it does not occur during the second and third cycle is that the time between cycles is insufficient for the oxide to convert into the soluble peroxide and hence deactivates the electrode for the remaining two cycles.

As for the anodic peak, the disappearance of the peaks when the potential range only covers the anodic range, shows that neither nitrate nor nitrite is the sole reactant of this oxidation reaction, since they are both available but the reaction does not take place in both melts. The reaction is dependent on a product of the reduction reaction. This validates the current literature understanding of the oxidation of the solid oxide produced on the electrode surface [20,21,23]. This is also validated by the fact that when the sweep range covers both ranges of the cathodic and anodic reactions, the anodic peak **A** reappears.

Nevertheless, compared to full range experiments in Section 3.1 with the two anodic peaks (**A1** and **A2**), for the range LV.c only one anodic peak (either **A1** or **A2**) occurs in the measurement. From the peak location, it is more probable it is **A2**. This could indicate that **A1** is related to another region of the CV that is not covered. There are two possibilities in this case. The first possibility is that **A1** is dependent on the cathodic limit (**CL**) at −3 V. Another possibility is that **A1** is the oxidation reaction of KO_2, and due to the reduced cathodic sweep range, KO_2 is not produced in the first place. KO_2 is known to require more negative potentials to be produced compared to Na_2O [21]. This could also be supported in the measurements in Figure S1 and Figure S2 in the Supplementary materials, which fall under the LV category but with extended ranges. The two peaks (**A1** and **A2**) appear if the cathodic sweep reaches the cathodic limit (**CL**). However, they do not appear if the anodic sweep reaches the anodic limit (**AL**).

As for the increase in the size of the peaks (**C** and **A2**) in second and third sweep cycle compared to the first cycle, it appears that there is an increase in the reduction capacity between the first and second cycle. Zambonin et at experienced a change in anodic peak size across scans, but it was due to adding a scan pause with different durations between cathodic and anodic peak, which allowed different dissolution of the solid oxide on the electrode surface [23]. However, the measurements presented here in this research did not use scan pauses and constant scan rates.

3.2.2. *Gas analysis combined with cyclic voltammetry*

In addition to the CV, another key observation considered in Section 3.2 is the gas production in each case as a result of the CV measurements. As noted previously, the gases produced at each electrode are physically separated by the experimental design, allowing differentiation between the gases generated at the working electrode and those generated at the counter electrode for each LV case.

No gas is produced at the working electrode for any of the three sweep ranges. Considering the gases produced at the counter electrode, when nitrite is added to the melt (comparing CE of Figs. 7 and Fig. 8), NO_2 disappears from the gas product. This is similar to the results of the FV category in Fig. 6 (a and c). Both the cathodic (LV.a) as well as the cathodic and anodic (LV.c) sweep show similar trends for the gas production in the eutectic melt (Fig. 7(a and c)); the NO production is higher than the NO_2 production.

The following is an attempt to correlate the gas production with the CV measurements. Most likely the gas production at the counter electrode in LV.a and LV.c cases is originating from the cathodic peak (**C**). The higher gas production for the combined peaks (LVc) could be related to the fact that the cathodic peak (**C**) appeared during all three sweep cycles, while it appeared only once in the isolated cathodic peak sweeps (LV.a, cycle 1).

On the other hand, it is believed in this work that no gas is produced at the anodic peak. One could argue that the increase in gas production (comparing case (c) to case (a) in Figs. 7 and Fig. 8) is related to the anodic peak which only appears in the LV.c sweep. However, the camera recording in this case supports the assumption that no gases are produced during the anodic peak at the counter electrode. Hence, whether the anodic peak is not produced (LV.b) or produced (LV.c), it is concluded that it produces no gases and that the anodic electrochemical

oxidation reaction is restricted to the melt.

Having established where and when the gases are produced, the focus now turns to their composition. These gases are believed to be generated at the counter electrode as a result of the cathodic peak (**C**). Accordingly, they are attributed to a half-cell reaction occurring at the counter electrode while the cathodic reduction reaction described in Eq. (3) takes place at the working electrode. Analysis of the gases produced at the counter electrode during the cathodic peak (**C**) shows that NO is the dominant product across all experiments. Bartlett et al. proposed an overall cell reaction corresponding to the half-cell reaction in Eq. (3) at peak (**C**) [19]. Although their work does not explicitly present the half-cell reaction occurring at the counter electrode, the overall cell reaction necessarily includes the products of the counter-electrode process. As indicated by the overall reaction in Eq. (10) [19], the gaseous products are NO_2 and O_2.

$$3\ NaNO_3 \rightarrow NaNO_2 + Na_2O + 2\ NO_2 + O_2 \quad (10)$$

This now appears to be inaccurate by the results of the experiments discussed here, as the reaction proposed by Bartlett et al. does not show NO in the products, which is actually the major compound produced near the counter electrode during the cathodic sweep. This suggests that NO is a product of an oxidation reaction happening simultaneously at the counter electrode when the nitrate reduction reaction occurs at the working electrode. Nevertheless, the behavior of the NO and NO_2 across the experiments will be discussed further in Section 3.4.

3.3. Constant voltage (Category cov)

The third and final category of the experiments is closely related to the second category. The most probable reason why only the first sweep cycle was successful during the cathodic sweep, is that the working electrode surface was deactivated by the metal oxide formed on it, which could also be observed through the window through the cell. Meanwhile, when no layer is formed on the working electrode, no oxidation can occur at the anodic peak; therefore, the anodic peak requires a preceding cathodic peak to occur.

Based on this hypothesis, this section focuses on the application of a constant potential corresponding to the maximum of peak (**C**) for 30 s and the subsequent analysis of the current response, a technique commonly referred to as chronoamperometry. Fig. 9 shows the current recorded when applying −1,6 V, which is where the cathodic peak appears, to the cell. The difference between the initial current of approximately −3 mA and the peak current of −40 mA reached in the complete CV curve (FV_Eu_N2) is unclear. Yet it could be due to a shift of the potential due to the quasi-reference electrode which does not allow for well-defined potentials. Nevertheless, it can still be seen that the initial current is high and then decreases over time until it reaches a very minimal constant value of −0,5 mA. This supports that the electrode is being deactivated, which is most likely through the formation of the metal oxide on the surface. On the other hand, when applying the same technique to the anodic peak (**A2**) at approximately −0,5 V, virtually no current was recorded to flow through the cell. This also supports the

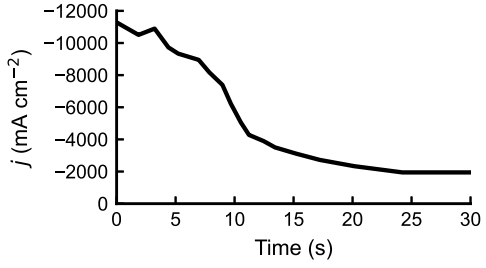

Fig. 9. Current measured by applying constant cathodic peak potential for 30 s (CoV_Eu_N2).

dependency of the anodic reaction on the cathodic reaction's products. The anodic peak reaction is an oxidation of the metal oxide deposited on the working electrode surface during the cathodic sweep, if it is not there, the anodic peak reaction will not take place.

Simultaneous to the constant voltage application, the gas can also be analyzed for each half cell chamber. This test was performed for both systems the eutectic melt (CoV_Eu_N2) and the 5 mol% nitrite melt (CoV_Nit_N2) and the results are presented in Fig. 10.

Similar results could be observed in this test to those from Section 3.2.

1. No gases are produced at the working electrode
2. The anodic reaction dependens on the cathodic reaction and does not take place if the cathodic reaction was not preceeded
3. NO_2 is not produced when nitrite is in the melt (Fig. 10(b), CE at cathodic peak potential)

The only major difference to the previous LV.a results is the ratio between the NO and NO_2 peak size at the counter electrode during the cathodic peak reaction (**C**) for the eutectic system Fig. 7(a). It appears that the NO_2 production has increased compared to the usual sweep (LV_Eu_N2). It still validates though that NO is produced at this potential, which is one major finding of this work.

3.4. Hypothetical phenomena

The hypothesis proposed in this work suggests that, during cyclic voltammetry in nitrate melts, not only electrochemical reactions occur during the potential sweeps, but additional chemical reactions also take place in both the molten medium and the gas phase, potentially altering the composition of the measured chemical species.

The hypothesis is as follows:

1. If NO_2 is detected in the system, it indicates that, NO and O_2 were initially produced electrochemically at the CE during the cathodic peak (**C**) and subsequently reacted in the gas phase to form NO_2. (Fig. 11(a))
2. If NO_2^- is present in the melt, it will react with the O_2 to form NO_3^-. (Fig. 11(b))

This hypothesis is supported by the discussion below, which focuses on the processes occurring at the counter electrode.

In the available literature, the previous work focused mainly on the working electrode side, whereas the present work considers both half-cell reactions. Although the counter electrode potential is not controlled during the cathodic sweep, characterizing the oxidation reactions there provides essential context for understanding the overall electrochemical process. Observing CE reactions could allow to propose a complete cell reaction, verify electron and mass balance, and better interpret the mechanism at the working electrode. This complementary perspective ensures that the working electrode half-reaction is considered within a coherent overall electrochemical framework, rather than in isolation.

The oxidation reaction at the counter electrode during the cathodic peak (**C**) produced in the present work NO as the major product. Nevertheless, the reaction indirectly proposed by Bartlett et al. [19], suggests NO_2 as the gaseous product. However, there has been no quantitative or definitive gas analysis performed. The formation of NO_2 is attributed to charge and atom balance considerations in a reversible electrochemical reaction and if only these are thermodynamically favorable.

The gas phase reaction in Eq. (11) always has to be considered when NO_2 and/or NO are produced in the presence of O_2 [30]. The reaction equilibrium can be calculated with listed thermodynamic values of the three gases [31].

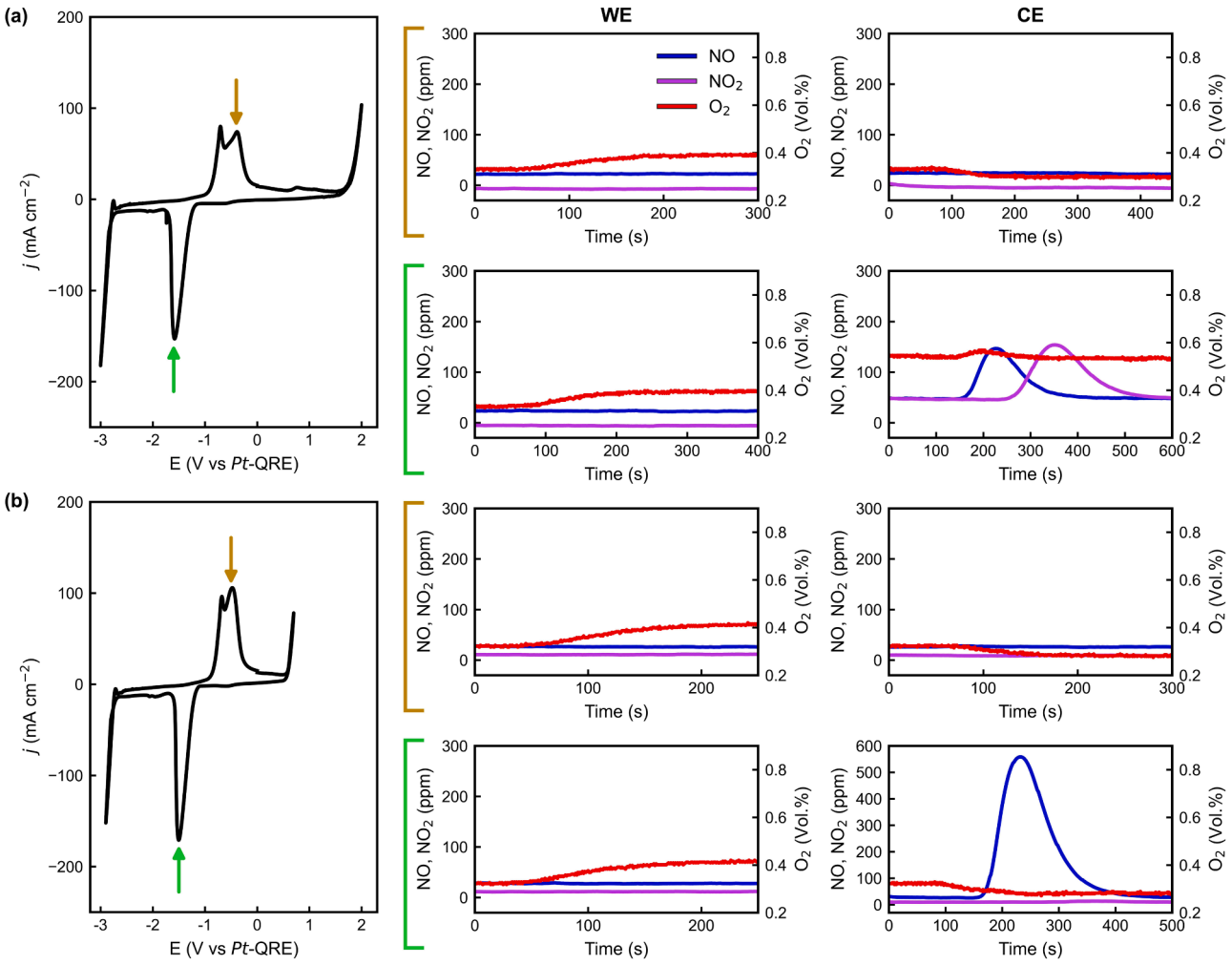

Fig. 10. Gas production (middle and right-hand side) during constant voltage application for 30 s at the cathodic and anodic peak potentials for (a) eutectic (CoV_Eu_N2) and (b) 5 mol% Nitrite melts (CoV_Nit_N2).

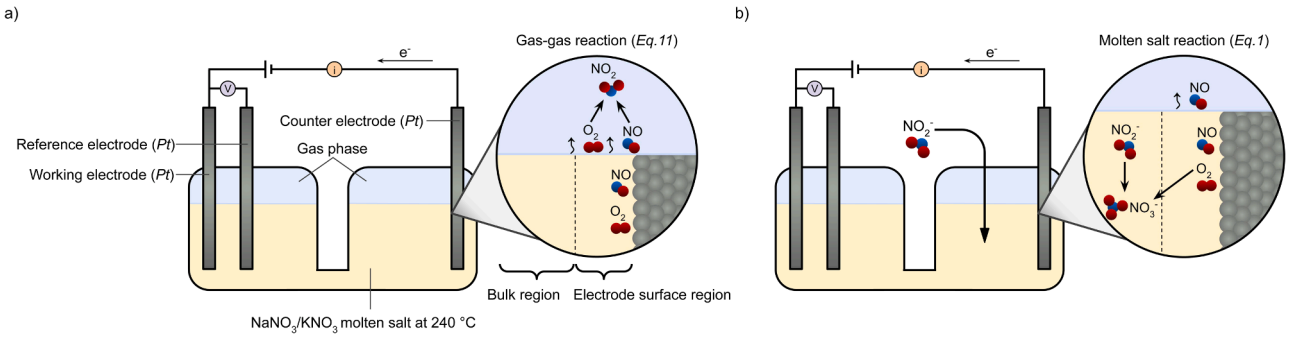

Fig. 11. Potential chemical reactions of the products of the cathodic peak (C) near the counter electrode: (a) Eutectic melt (b) 5 mol% Nitrite melt.

$$NO + 1/2\ O_2 \rightleftarrows NO_2 \quad (11)$$

Below 350 °C, nitrogen dioxide predominates, whereas nitrogen monoxide predominates above 500 °C [32]. This means, that at the temperature used for these experiments (240 °C), it is likely that NO_2, which is seen in the gas analysis, is a product of the reaction of electrochemically produced NO and O_2. Either on the electrode surface or in the gas phase. The latter case is illustrated in Fig. 11(a) below. This hypothesis is further supported by the increase of NO_2/NO ratio when oxygen gas is introduced in the gas phase (FV_Eu_O2N2). Here, the more available O_2 for the gas phase reaction shifts the gas equilibrium further towards the NO_2 side.

Furthermore, the hypothesis is also supported by the results of the measurements of the 5 mol% nitrite salt, which all show absence of NO_2 in the product under nitrogen atmosphere (FV_Nit_N2 in Fig. 6(c) and LV_Nit_N2 in Fig. 8(a and c)). The sudden presence of oxygen near the electrode in a melt environment that includes nitrite, would shift the equilibrium of the reaction in Eq. (1) towards the nitrate side, as at this temperature virtually no nitrite is expected to be present in the melt at equilibrium [33]. Hence, as depicted in Fig. 11(b), with the availability of both components of the reaction – nitrite and oxygen – they would

immediately react into nitrate. As a result, there is no remaining oxygen for the gas phase reaction to convert NO into NO_2. This is again also supported by the reappearance of the NO_2 peak when O_2 is introduced in the gas stream for the 5 mol% nitrite salt complete cycle measurement (FV_Nit_O2N2), as there is excessive O_2 available for the gas phase reaction.

It is also unlikely that the anodic limit generates NO_2 via Eqs. (7) and (8), as suggested in the literature, because this contradicts the observed disappearance of NO_2 from the product gas of a full range sweep under a nitrogen atmosphere (FV_Nit_N2) in Fig. 6(c). This interpretation is further supported by a comparison of Figures S3 and S4 in the Supplementary Materials, where the potential sweep ranges include only the anodic limit. In these experiments, NO is the dominant gaseous product for both the eutectic and the 5 mol% nitrite melts. The differences in gas products reported in the literature could be influenced by variations in electrode design, particularly the relative size of the counter electrode, which governs the local current density and thus the reaction pathways. A systematic investigation of electrode geometry could clarify its role in gas evolution behavior.

4. Conclusion

This work provided an opportunity to study the gases produced at the working and counter electrode using two half-cells during cyclic voltammetry in potassium-sodium nitrates eutectic at 240 °C. In addition, salt analysis and visual inspection was performed. The main results are:

- Differences in the salt composition could not be identified within the measurement uncertainty and could potentially be detected in future studies through adjustments, such as longer experiment durations or redesigning the salt bridge.
- At the working electrode, a translucent layer is visible on the electrode at cathodic peak (**C**), which dissolves at the anodic peaks (**A1** and **A2**) and excessive gas production is to be seen at the anodic limit (visual inspection).
- At the counter electrode gas production is visible at cathodic peak (**C**) and cathodic limit (**CL**), while the latter is excessive (visual inspection).
- No gases are produced during the anodic peaks (visual inspection and gas analysis).
- No gases are produced near the working electrode at the cathodic peak (**C**) (visual inspection and gas analysis).
- The major gas product at the counter electrode is NO (gas analysis).
- NO_2 appears in the product gas as a secondary product for eutectic melt, but does not appear when the melt includes 5 mol% nitrite (gas analysis).
- The cathodic peak (**C**) is not reproducible during the second and third sweep cycle if the sweep range does not reach the anodic peak potential (cyclic voltammetry).
- The anodic peaks (**A1** and **A2**) are dependent on the cathodic sweep (cyclic voltammetry)

The findings allow conclusions regarding the stable operating window of nitrate systems with and without nitrite:

- the narrowest reversible operating window exists between **C** and **AL** without transformation, with currents at **C** minimized to reduce oxide formation on the electrode.
- The anodic limit (**AL**) depends on the nitrite content; adding nitrite reduces the operating window.

By deliberately restricting the experiments to three voltage ranges, the relationship between the cathodic and anodic peaks could be investigated more precisely, yielding the following conclusions:

- The formation of the sparingly soluble sodium oxide at the cathodic peak on the working electrode, as suggested in the literature, could be verified through various cyclic voltammetry ranges and visually confirmed in this study. The electrode is deactivated through the oxide deposition and needs the anodic peak(s) (**A1** and **A2**) to be regenerated. Furthermore, pausing the experiment allowed the reactivation of the electrode passivated by oxides, indicating a dissolution of the poorly soluble oxide species when converted to the more soluble species.
- This work demonstrates, using the half-cell setup with gas analysis, that NO is produced at the counter electrode during the cathodic peak, whereas the literature so far assumes mainly NO_2 formation.
- Based on that, a hypothesis suggests that NO and O_2 are produced at the counter electrode during the cathodic peak (**C**), which would behave differently based on the melt composition:
  - Eutectic: NO and O_2 react and produce NO_2 **in the gas phase**
  - 5% mol Nitrite: O_2 reacts with NO_2^- **in the melt** and only NO is produced as gas

CRediT authorship contribution statement

Nada Zaghloul: Writing – original draft, Visualization, Validation, Methodology, Investigation, Formal analysis, Data curation, Conceptualization. **Ekin Zehra Metin:** Writing – review & editing, Visualization. **Markus Braun:** Writing – review & editing, Methodology, Investigation, Conceptualization. **Thomas Bauer:** Writing – review & editing, Validation, Supervision, Conceptualization.

Declaration of competing interest

The authors declare that they have no known competing financial interests or personal relationships that could have appeared to influence the work reported in this paper.

Supplementary materials

Supplementary material associated with this article can be found, in the online version, at doi:10.1016/j.electacta.2026.148808.

Data availability

Data will be made available on request.

References

[1] T. Bauer, C. Odenthal, A. Bonk, Molten salt storage for power generation, Chem. Ing. Tech. 93 (4) (2021) 534–546, https://doi.org/10.1002/cite.202000137.
[2] M. Mehos, et al., Concentrating solar power best practices study, Natl. Renew. Energy Lab.(NREL) (2020). Solar Dynamics LLC.
[3] C.S. Turchi, J. Vidal, M. Bauer, Molten salt power towers operating at 600–650 C: salt selection and cost benefits, Sol. Energy 164 (2018) 38–46, https://doi.org/10.1016/j.solener.2018.01.063.
[4] A.M. Kruizenga, D.D. Gill, and M.E. LaFord, "Corrosion of High Temperature Alloys in Solar Salt at 400, 500, and 680ÀC," United States, 2013. [Online]. Available: https://www.osti.gov/biblio/1104752.
[5] K.H. Stern, High temperature properties and decomposition of inorganic salts part 3, nitrates and nitrites, J. Phys. Chem. Ref. Data 1 (3) (1972) 747–772, https://doi.org/10.1063/1.3253104.
[6] V.A. Sötz, A. Bonk, J. Steinbrecher, T. Bauer, Defined purge gas composition stabilizes molten nitrate salt-experimental prove and thermodynamic calculations, Sol. Energy 211 (2020) 453–462, https://doi.org/10.1016/j.solener.2020.09.041.
[7] B. Bond, P. Jacobs, The thermal decomposition of sodium nitrate, J. Chem. Soc. A: Inorg. Phys. Theor. (1966) 1265–1268, https://doi.org/10.1039/J19660001265.
[8] R.W. Bradshaw et al., "Final test and evaluation results from the solar two project," Sandia National Lab.(SNL-NM), Albuquerque, NM (United States); Sandia …, 2002.
[9] R.F. Bartholomew, A study of the equilibrium KNO3 (l) ⇄ KNO2 (l)+ 1/2O2 (g) over the temperature range 550-750, J. Phys. Chem. 70 (11) (1966) 3442–3446.
[10] G. Picard, H. Lefebvre, B. Trémillon, Thermodynamic study of corrosion of iron in NaNO3-NaNO2 mixtures, J. Electrochem. Soc. 134 (1) (1987) 52, https://doi.org/10.1149/1.2100435.
[11] A. Gomes, M. Navas, N. Uranga, T. Paiva, I. Figueira, T.C. Diamantino, High-temperature corrosion performance of austenitic stainless steels type AISI 316L and

AISI 321H, in molten Solar Salt, Sol. Energy 177 (2019) 408–419, https://doi.org/10.1016/j.solener.2018.11.019.
[12] Q. Gong, W. Ding, Y. Chai, A. Bonk, J. Steinbrecher, T. Bauer, Chemical analysis and electrochemical monitoring of extremely low-concentration corrosive impurity MgOHCl in molten MgCl2–KCl–NaCl, Front. Energy Res. 10 (2022) 811832, https://doi.org/10.3389/fenrg.2022.811832.
[13] C. Zhang, D. Rappleye, A. Nelson, S. Simpson, M. Simpson, Electroanalytical measurements of oxide ions in molten CaCl2 on W electrode, J. Electrochem. Soc. 168 (9) (2021) 097502, https://doi.org/10.1149/1945-7111/ac208e.
[14] F. Felling, O.R. Dale, M. Gonzalez, C. Zhang, M.F. Simpson, Application of cyclic voltammetry with W electrodes for measurement of high CaO concentration in molten CaCl2, J. Electrochem. Soc. 171 (1) (2024) 017514, https://doi.org/10.1149/1945-7111/ad1eca.
[15] L. Massot, L. Cassayre, P. Chamelot, P. Taxil, On the use of electrochemical techniques to monitor free oxide content in molten fluoride media, J. Electroanal. Chem. 606 (1) (2007) 17–23, https://doi.org/10.1016/j.jelechem.2007.04.005.
[16] H. Qiao, T. Nohira, Y. Ito, Electrochemical behavior of oxide ion at a glassy carbon electrode in a LiF-NaF-KF eutectic melt, Electrochemistry 71 (7) (2003) 530–535, https://doi.org/10.5796/electrochemistry.71.530.
[17] S. White, U. Twardoch, The solubility and electrochemistry of alkali metal oxides in the molten eutectic mixture of lithium carbonate-sodium carbonate-potassium carbonate, J. Appl. Electrochem. 19 (6) (1989) 901–910, https://doi.org/10.1007/BF01007939.
[18] N. Elgrishi, K.J. Rountree, B.D. McCarthy, E.S. Rountree, T.T. Eisenhart, J. L. Dempsey, A practical beginner's guide to cyclic voltammetry, J. Chem. Educ. 95 (2) (2018) 197–206, https://doi.org/10.1021/acs.jchemed.7b00361.
[19] H. Bartlett, K. Johnson, Cathode processes in molten nitrates and nitrites, J. Electrochem. Soc. 114 (1) (1967) 64, https://doi.org/10.1149/1.2426508.
[20] I. Singh, S. Sultan, K. Balakrishnan, Cyclic voltammetric behaviour of platinum in dried and wet nitrates melt, Electrochim. Acta 38 (17) (1993) 2611–2615, https://doi.org/10.1016/0013-4686(93)80159-W.
[21] M. Miles, A. Fletcher, Cation effects on the electrode reduction of molten nitrates, J. Electrochem. Soc. 127 (8) (1980) 1761, https://doi.org/10.1149/1.2129996.
[22] V. Villard, H. Lefebvre, D. Ferry, G. Picard, Voltammetric investigations of the oxygen electrochemical systems in molten sodium nitrate at 420 °C, Electrochim. Acta 33 (4) (1988) 545–549, https://doi.org/10.1016/0013-4686(88)80175-0.
[23] P.G. Zambonin, Oxide chemistry and electroreduction of NO3− in molten alkali nitrates, J. Electroanal. Chem. Interfacial. Electrochem. 24 (2–3) (1970) 365–377, https://doi.org/10.1016/S0022-0728(70)80159-0.
[24] H.S. Swofford, H. Laitinen, An electrochemical investigation of the reduction of nitrate in NaNO3-KNO 3 eutectic at 250 °C, J. Electrochem. Soc. 110 (7) (1963) 814, https://doi.org/10.1149/1.2425878.
[25] H. Swofford, P. McCormick, An electrochemical study of nitrite and oxide in sodium nitrate-potassium nitrate eutectic melts, Anal. Chem. 37 (8) (1965) 970–974, https://doi.org/10.1021/ac60227a005.
[26] D.L. Manning, Voltammetry of silver in molten sodium nitrate-potassium nitrate: use of a controlled-potential polarograph and a platinum quasi-reference electrode, Talanta 10 (3) (1963) 255–260, https://doi.org/10.1016/0039-9140(63)80226-X, 1963/03/01/.
[27] J. Steinbrecher, A. Bonk, V.A. Sötz, T. Bauer, Investigation of regeneration mechanisms of aged solar salt, Mater. (Basel) 14 (19) (2021) 5664, https://doi.org/10.3390/ma14195664.
[28] K. Johnson, P. Zacharias, J. Matthews, Oxygen ions in individual nitrate melts, ECS Proc. Vol. 1976 (1) (1976) 603, https://doi.org/10.1149/197606.0603PV.
[29] I. Singh, S. Sultan, K. Balakrishnan, Cathodic process on iron in NaNO3 and KNO3 melts, Electrochim. Acta. 40 (11) (1995) 1755–1759, https://doi.org/10.1016/0013-4686(95)92647-X.
[30] R.I. Olivares, W. Edwards, LiNO3–NaNO3–KNO3 salt for thermal energy storage: thermal stability evaluation in different atmospheres, Thermochim. Acta 560 (2013) 34–42, https://doi.org/10.1016/j.tca.2013.02.029, 2013/05/20/.
[31] I. Barin, La-Lu2O3, Thermochemical data of Pure Substances, Wiley-VCH, Verlag GmbH, 2008.
[32] L. Olsson, B. Westerberg, H. Persson, E. Fridell, M. Skoglundh, B. Andersson, A kinetic study of oxygen adsorption/desorption and NO oxidation over Pt/Al2O3 catalysts, J. Phys. Chem. B 103 (47) (1999) 10433–10439, https://doi.org/10.1021/jp9918757, 1999/11/01.
[33] D. Nissen, D. Meeker, Nitrate/nitrite chemistry in sodium nitrate-potassium nitrate melts, Inorg. Chem. 22 (5) (1983) 716–721, https://doi.org/10.1021/ic00147a004.